QRS DETECTION ALGORITHMS: A STUDY OF PERFORMANCE

دراسة لأداء خوارزمات التعرف على موجات QRS

F.E.Z. Abou-Chadi, H. S. Ragab, and H. H. Soliman
Department of Electronics and Communications Engineering,
Faculty of Engineering- Mansoura University

الخلاصة– هذا البحث يقدم دراسة مقارنة لأداء عدد سبعة عشر خوارزما للتعرف على أزمنة حدوث موجات QRS. وقد تم تصميم نظام للتقييم يقوم بمقارنة الأداء بدلالة دقة تحديد زمن الحدوث ومدى إعتماد الخوارزم على شكل الموجات المراد تعيينها. وقد تم تعيين دقة زمن الحدوث باستخدام أسلوب المحاكاة حيث أمكن إنتاج عدد من إشارات رسم القلب الكهربى وإضافة نسب معينة من الأنواع المختلفة والمحاكية للشوشرة التى عادة ما تختلط بإشارات رسم القلب. أما لتحديد مدى إعتماد الخوارزم على شكل نبضات QRS فقد تم استخدام عدة تسجيلات لقاعدة البيانات القياسيةAHA. وقد أظهرت النتائج أن الخوارزمات التى تعتمد على المفاضلات الرقمية تكون حساسة للتغيرات التى تحدث فى خط الأساس للإشارة وأيضا للشوشرة ذات الترددات المرتفعة مثل تلك التى تنتج من انشاط الكهربى للعضلات. أما الخوارزمات التى تعتمد على المرشحات الخطية واللاخطية فهى قادرة على تعيين جميع النبضات ولكن مع حدوث تقديم أو تأخير فى أزمنة الحدوث. وقد أعطت الخوارزمات التى تعتمد على الشبكات العصبية وتحويل المويجة wavelet أعلى أداء وبخاصة الخوارزم الذى يعتمد على شبكة العصبية الخطية. فهو أقلهم حساسية لجميع أنواع الشوشرة ولايعتمد فى أدائه على شكل موجات QRS سواء فى الحالات العادية أوالمرضية ولايسبب اى تقديم او تأخير فى أزمنة الحدوث.

Abstract- A detailed comparison of the performance of seventeen different QRS detection algorithms under noise conditions is undertaken. An evaluation scheme is developed to compare the detection performance in terms of timing accuracy and reliability. These include identification of the number of detected beats, the number of false positives, the number of false negatives, the number of multiple detection, the time delay and time advance. The use of a synthesized ECG signal allowed the timing reference for the QRS complex to be known. For QRS detection reliability tests, records from the standard American Heart Association Database (AHA) were used as test signals. It has been concluded that algorithms based on amplitude and first derivative give high performance for ECG corrupted with EMG noise but are sensitive to changes in baseline drift which accounts for the decrease in performance when subjected to composite noise. Algorithms based on first, first and/second derivatives overcome the baseline wandering, however, their performance is affected by the high frequency noise e.g. EMG. Algorithms based on linear and nonlinear filtering detects the correct number of beats but with time advance and time delay due to the filter phase characteristics. Algorithms based on neural network and wavelet neural network gave the highest performance. Specifically, an algorithm based on wavelet neural network is the most insensitive to all types of noise, and is the most reliable to detect QRS complexes under all types of abnormalities with no time advance or delay.

Received September 27, 1998

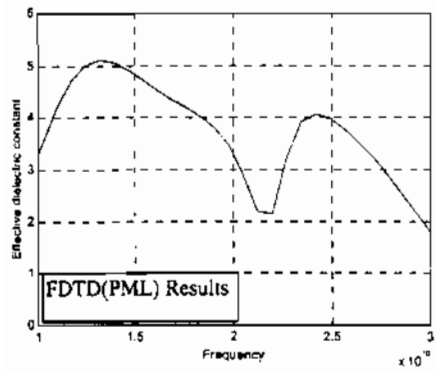

Fig. 11 Effective dielectric constant.

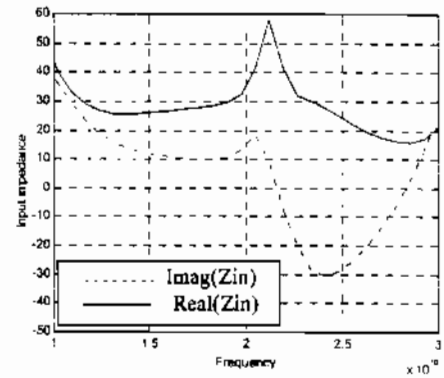

Fig. 12. The input impedance at a $12\Delta x$ from the via

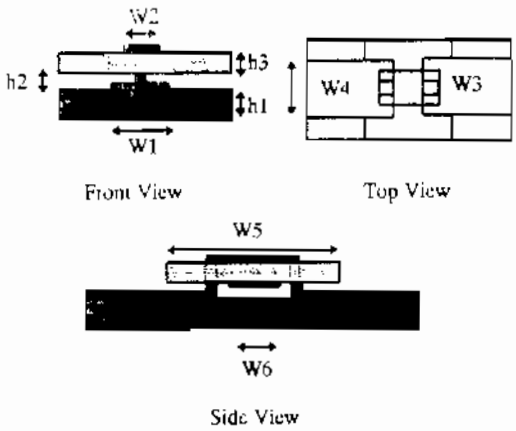

Fig. 8. Double-via-transition package. The bottom and top layers have dielectric constants of 2.2 and 6.2, respectively. (h1=0.8 mm, h2=0.4 mm, h3=0.6 mm, w1=2.4 mm, w2=0.8 mm, w3=0.4 mm, w4=5.2 mm, w5=0.8 mm, w6=3.6 mm, and t=0.2mm)

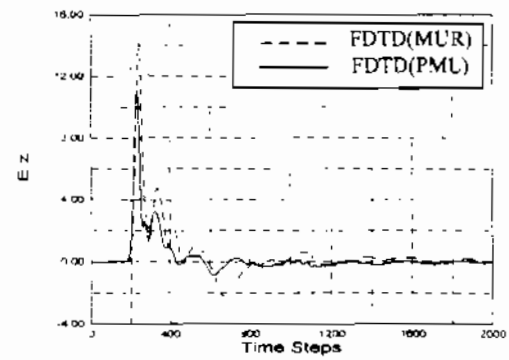

Fig. 9. The transmitted and reflected signals (solid with PML and dashed with MUR) (12 Δx from the begging of the via)

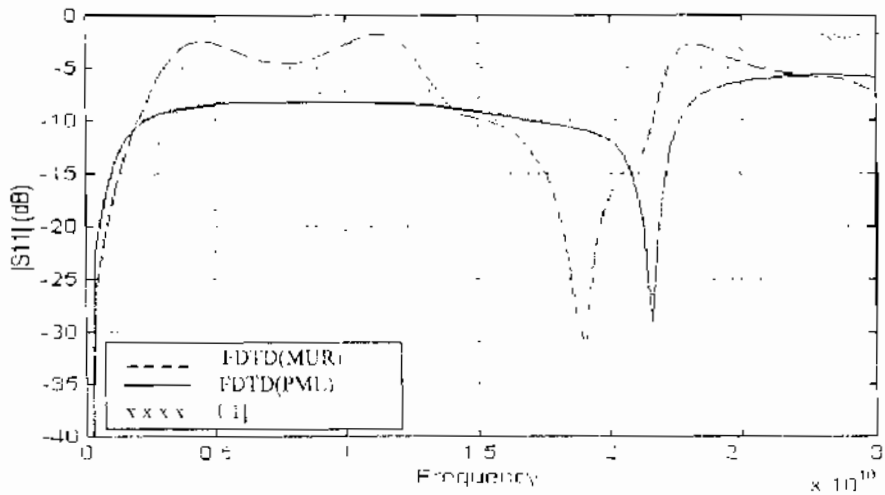

Fig. 10. The S11 versus frequency for double-via-transmission package.

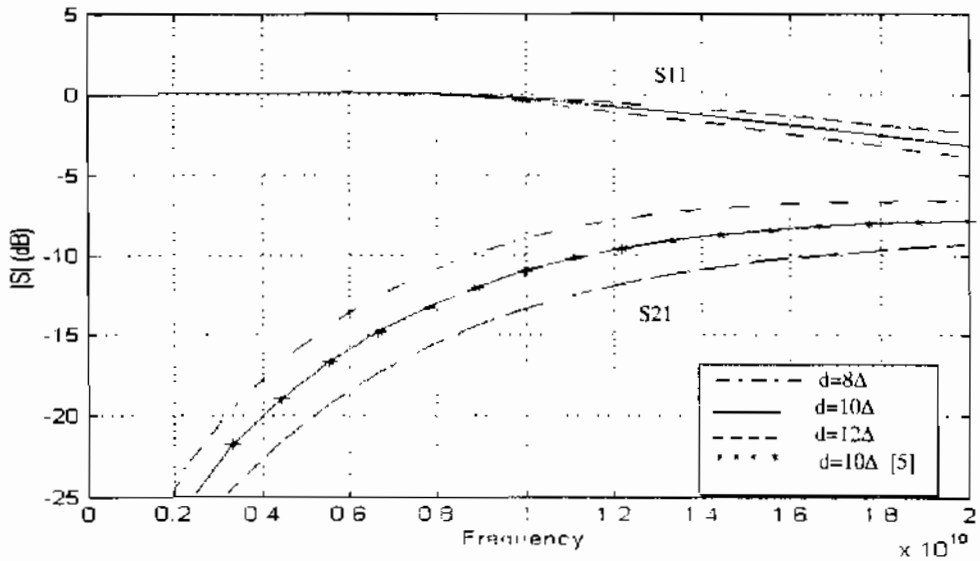

Fig. 4 The scattering parameters obtained with FDTDM with PML ABC's.

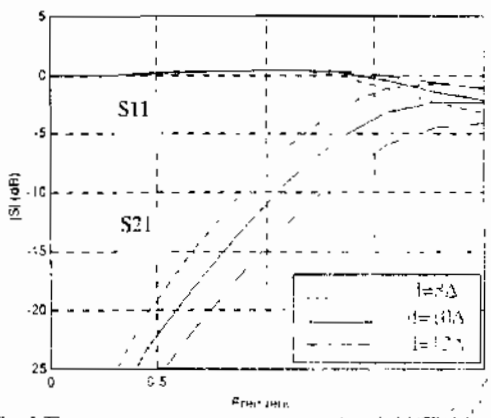

Fig. 5 The scattering parameters [illegible]
with MUR's 1D

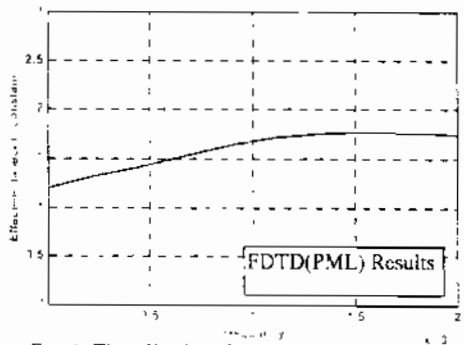

Fig. 6 The effective dielectric constant (PML)

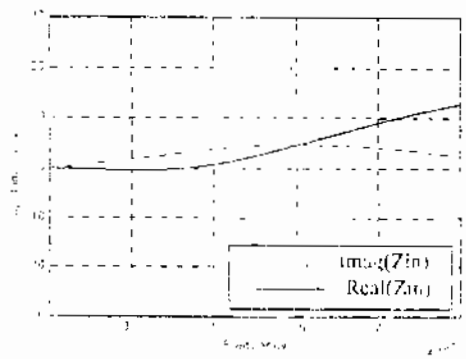

Fig. 7 The Normalized input [illegible]

effective dielectric constant, and normalized input impedance are obtained. The present results are compared with the published data and good agreement has been found.

References

[1] A. C. Polycarpou, P. A. Tirkas, and A. Balanis, "The finite-element method for modeling circuits and interconnects for electronic packaging," IEEE Trans. Microwave Theory Tech., vol. 45, pp. 1868-1874, Oct. 1997.

[2] W. Heinrich, A. Jentzsch, and G. Baumann, " Millimeter-wave characteristics of flip-chip interconneets for multichip modules," IEEE Trans. Microwave Theory Tech., vol. 46, pp. 2264-2268, Dec. 1998.

[3] J. Wee, Y. Park, H. Min, D. Cho, M. Seung, and H. Park, " Modeling the substrate effect in interconnect line characteristics of high-speed VLSI circuits," IEEE Trans. Microwave Theory Tech., vol. 46, pp. 1426-1443, Oct. 1998.

[4] W. Becker, P. Harms, and R. Mittra, " Time-domain electromagnetic analysis of interconnects in a computer ehip packaging," IEEE Trans. Microwave Theory Tech., vol. 40, pp. 2155-2163, Dec. 1992.

[5] D. Koh, H,. Lee, and T. Itoh, " A hybrid full-wave analysis of via-hole grounds using fiuite-difference and finite element time-domain methods," IEEE Trans. Microwave Theory Tech., vol. 45, pp. 2217-2223, Dec. 1997.

[6] Mur G., " Absorbing bonndary conditions for the finite-difference approximation of the time-domain, electromagnetic field equations," IEEE Trans., Electromagnetic Compat., vol. 23, no. 4, pp.377 - 382, Nov. 1981.

[7] Jean -Pierre Berenger, " A perfectly matched layers for the FDTD solntion of wave-structnre interaction problems," IEEE Trans. Antenna and Propagat. vol. AP-44, pp. 110-117, Jan. 1996.

[8] Karl, S. Kuenz and Raymonnd J. Luebbers, The Finite- Difference Time - Domain Method for Electromagnetics CRC press, London Tokyo, 1993.

[9] R. Mittra, and U. Pekel, " A new look at the perfect matched layer (PML) concept for the reflectionless absorption of electromagnetic waves," IEEE Microwave and Guided Wave Letters vol.5, no.3, pp. 84-86, march 1995.

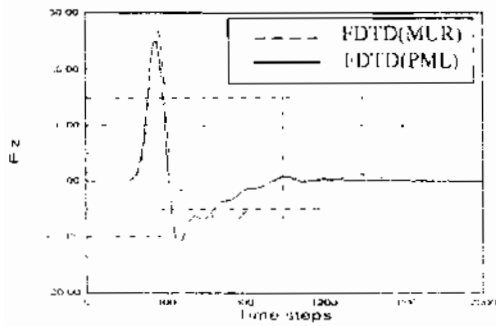

Fig. 2 The total (incident and reflected) wave at the reference plane on the via-hole grounded microstrip.

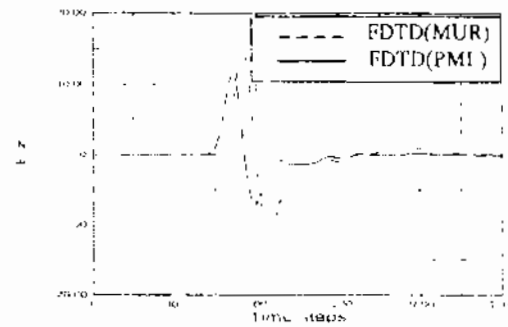

Fig. 3 The transmitted wave at the output port on the via-hole grounde Microstrip.

III. Numerical Results

Extensive numerical simulations based on a three dimensional FDTD technique have been conducted for two different types of practical electronic packaging. In addition, the effect of using the recently developed Berenger PML ABC's is studied.

The first analyzed structure is shown in Fig. 1. It represents a via-hole grounded microstrip line with a via hole diameter of 0.6 mm, microstrip width 2.3 mm, a substrate of thickness 0.794 mm, and dielectric constan 2.32 [5]. According to criterion stability condition , equation (3), a Yee cell of $\Delta x=\Delta y=\Delta z=0.0575$ mm was considered. This leads to discretize the computational domain by 60x20x100 FDTD cells. The excitation is taken as a Gaussian pulse with f_{max}=20 GHz. The reference plane is defined 18 Δx away from the begging of the via hole while the output port is taken 5 Δx from the end of the microstrip. The via is taken as a cylinder and the staircasing technique is used to model the via-bole boundary [5]. Fig. 2 and Fig .3 show the incident, reflected, and transmitted signals on the line. To separate the incident and reflected signals in Fig. 2, two simulations are carried out. The first with the presence of the discontinuity which give the total (incident and reflected) wave at the reference plane. The second is carried out with the absence of the discontinuity which give only the incident wave at the reference plane. Using the two simulations, the incident and reflected wave forms can be obtained. By applying the Fourier transformation to the incident, reflected, and transmitted waves, one can calculate the scattering parameters [1]. Figure 4 and Figure 5 show the scattering parameters for both types of ABC's. Comparing the obtained results with those of Kon, et. al. [5] which were obtained by FDTD with super ABC's of MUR, it is found that these results are in better agreement with our results obtained with PML. The effect of changing the via diameter is shown in these figures. These figures show that increasing the via hole diameter leads to decrease the scattering parameters [5]. The effective dielectric constant and the input impedance are shown in Fig. 6 and Fig.7, respectively. Fig. 6 shows that as the frequency goes up, the effective dielectric constant tends to a value equal to the relative dielectric constant of the substrate. In calculating the input impedance, the characteristic impedance of the microstrip line is assumed to be equal 50Ω.

The second numerical example is the double- via-transition package which is shown in Fig. 8. In this case the Yee cell has Δx=0.2 mm , Δy=0.1 mm, and Δz=0.1 mm [1]. The excitation is taken as a Gaussian pulse with f_{max}=30 GHz. The reference plane is defined at 12 Δx away from the begging of the via. Fig. 9 shows the time domain response while Fig. 10 shows the magnitude of S11. The scattering parameter (S11) is compared with that obtained by FEM [1] with MUR ABC's. Good determination of the location of the resonance frequency is obtained by using the PML ABC's. Fig. 11 and Fig. 12 show the effective dielectric constant and the input impedance, respectively. From the last figure, it has found that at the resonance frequency, the imaginary part of the input impedance goes to zero while its real part makes minimum value; i.e. the circuit acts as a series resonance circuit.

IV. Conclusion

The FDTD has been conducted to the analysis of practical microwave electronic packaging. PML and MUR ABC's are used to terminate the FDTD cell meshes. With PML ABC's, more accurate results are obtained due to the better elimination of the nonphysical reflections of the ABC's to the computational domain. Results for the time domain response, scattering parameters,

where Δx, Δy, and Δz are the spatial increments in the x, y, and z directions, respectively. The C's and D's coefficients are as given in detail in reference [8].

For a non-homogeneous domain, each homogeneous region is treated separately and then the boundary conditions are forced at the interfaces.

To ensure that the numerical error generated in one calculation step does not accumulate and grow, the stability criterion of Yee's algorithm relating Δ_x, Δ_y, and Δ_z and Δt is applied [8],

$$\Delta t \le \frac{1}{v_c}\left(\frac{1}{\Delta x^2}+\frac{1}{\Delta y^2}+\frac{1}{\Delta z^2}\right)^{-\frac{1}{2}} \tag{3}$$

where

Δt is the maximum time step that may be used, and
V_c is the phase velocity in the medium.

B. Perfectly Matched Layer PML

The PML is a nonphysical absorber adjacent to the outer boundary of the computational domain for an open structure. The PML ensures that a plane wave incident at any arbitrary angle or frequency from the free-space upon a PML region is totally transmitted into the PLM region with negligible reflections toward the inner structure [7]; i.e. total absorption for the outgoing waves. This is carried out by introducing an additional degree of freedom by splitting the field components with anisotropic material properties in the PML region. For this material, the electric conductivity and the magnetic loss is related by [7],

$$\frac{\sigma}{\varepsilon_o}=\frac{\sigma^*}{\mu_o} \tag{4}$$

where σ^* denotes the magnetic conductivity.

Theoretically, for a layer of such conductivities there is no reflections from the inner sides of the PML region to the inner structure (computational domain). However, the outgoing waves are reflected by the perfectly conducting conditions at the outer boundary of the PML region and may be returned to the inner domain. Berenger [7] suggested a conductivity profile($\sigma(\rho)$); ρ is the distance from the inner interface) which provides the decay of the outgoing field to zero as it goes to the outer boundaries. This totally eliminates reflections from the onter boundary of the PML to the inner structure. Accordingly, Maxwell's equations can be written as [9],

$$\mu_o\frac{\partial H_{xy}}{\partial t}+\sigma_y^* H_{xy}=-\frac{\partial\left(E_{zx}+E_{zy}\right)}{\partial y} \tag{5.a}$$

$$\mu_o\frac{\partial H_{xz}}{\partial t}+\sigma_z^* H_{xz}=\frac{\partial\left(E_{yx}+E_{yz}\right)}{\partial z} \tag{5.b}$$

$$\varepsilon_o\frac{\partial E_{xy}}{\partial t}+\sigma_y E_{xy}=\frac{\partial\left(H_{zx}+H_{zy}\right)}{\partial y} \tag{6.a}$$

$$\varepsilon_o\frac{\partial E_{yz}}{\partial t}+\sigma_z E_{yz}=-\frac{\partial\left(H_{xx}+H_{xz}\right)}{\partial z} \tag{6.b}$$

different types of absorbing boundary conditions are used to terminate the FDTD meshes; Mur first order [6] and Berenger perfectly matched layer (PML) [7]. Numerical results for the time domain response, scattering parameters, effective dielectric constant, and input impedance are obtained. Good agreement with the available published data for the scattering parameters is found.

II. Formulation of the Problem

A. Time Domain Finite Difference Formulation

The via-hole grounded microstrip line is shown in Fig. 1 where the strips and the bottom planes are made of perfectly conducting material. The substrate has a relative dielectric constant ε_r. The microstrip line is taken as an open structure. For this structure, Maxwell's equations can be written as:

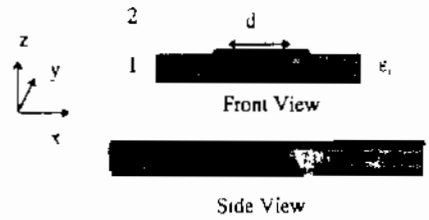

Fig.1 The via-hole grounded microstrip.

$$\frac{\partial \bar{H}_i}{\partial t} = -\frac{1}{\mu_i}\nabla x \bar{E}_i - \frac{\rho_i}{\mu_i}\bar{H}_i \tag{1.a}$$

$$\frac{\partial \bar{E}_i}{\partial t} = \frac{1}{\varepsilon_i}\nabla x \bar{H}_i - \frac{\sigma_i}{\varepsilon_i}\bar{E}_i \tag{1.b}$$

where,

ρ : is the magnetic resistivity of the medium in (Ω/m)

σ : is the electric conductivity of the medium in (S/m)

i=1,2 represents the substrates and free space, as shown in the Fig.1.

To discretize Maxwell's equations (1.a) and (1.b), the centered difference approximation is applied to both time and space first-order partial differentiations. Following Yee [8], one can get the discretized Maxwell's equations for homogeneous regions as follows [8]:

$$H_x\Big|_{i,j,k}^{n+1/2} = D_a\Big|_{i,j,k} H_x\Big|_{i,j,k}^{n-1/2} + D_b\Big|_{i,j,k} \left\{ \frac{E_z\Big|_{i,j+1,k}^{n} - E_z\Big|_{i,j,k}^{n}}{\Delta z} - \frac{E_y\Big|_{i,j,k+1}^{n} - E_y\Big|_{i,j,k}^{n}}{\Delta y} \right\} \tag{2.a}$$

$$E_x\Big|_{i,j,k}^{n+1} = C_a\Big|_{i,j,k} E_x\Big|_{i,j,k}^{n} + C_b\Big|_{i,j,k} \left\{ \frac{H_z\Big|_{i,j,k}^{n+1/2} - H_z\Big|_{i,j-1,k}^{n+1/2}}{\Delta y} - \frac{H_y\Big|_{i,j,k}^{n+1/2} - H_y\Big|_{i,j,k-1}^{n+1/2}}{\Delta z} \right\} \tag{2.b}$$

A Finite Difference Time Domain Analysis of Microwave Electronic Packaging

تحليل المعلبات الإليكترونية الميكروووية باستخدام طريقة الفروق المحدودة فى الحيز الزمنى

Maher M. Abd Elrazzak, *Member, IEEE*
Faculty of Eng., Mansoura Univ., Mansoura, Egypt.
email: maher@ieee.org

فى هذا البحث تم استخدام طريقة الفروق المحدودة فى الحيز الزمنى (FDTD) لتحليل المعلبات الإليكترونية الميكروووية مع استخدام شروط حدية ماصة من نوع الطبقات المتوائمة تماما لبرينجر (Berenger's PML) وكذلك شروط مير من الدرجة الأولى(Mur's FOC) . ولهذه المعلبات تم حساب المجال فى الحيز الزمنى (Time domain field response) . بارامترات التشتت (Scattering parameters) والمعاوقة الداخلية (input impedance) و ثابت العزل الفعال (Effective dielectric constant). و كذلك تم دراسة تأثير تغير طول قطر فتحات الاتصال على بارامترات التشتت الخاصة بهذه المعلبات.

وقد وجد أن النتائج التى تم الحصول عليها بطريقة الفروق المحدودة فى الحيز الزمنى مع إستخدام الطبقات تامة المواءمة أكثر دقة من النتائج المنشورة و المحسوبة أيضا بنفس الطريقة مع استخدام شروط الامتصاص الحدية لمير ذات الدرجة الأولى.

Abstract- Time-frequency domain analysis of practical microwave electronic packaging is presented. This analysis is based on the finite difference time domain (FDTD) with two different types of absorbing boundary conditions: MUR first order and Berenger perfectly matched layer (PML). The method is used to calculate the time domain response, the scattering parameters, the effective dielectric constant, and the input impedance. In addition, the effect of the via hole diameter on the scattering parameters is studied. The obtained results are compared with the available published data for the scattering parameters and better accuracy is found.

I. Introduction

The time and frequency domains analysis of interconnects for electronic packaging represent a critical analysis and design problem of high-speed integrated very large scale integration (VLSI) circuits. This is to minimize the signal distortion due to the propagation loss and dispersion. The latters usually appear at high-frequency operation and lead to strong coupling and interference among neighboring transmission lines of the package [1-4]. In addition, parasitic effects such as radiation and time delay may result due to the different discontinuities in the package; metallic bridges, bond wires, microstrip bends, and the cond[illegible] [5].

In the present work, a full wave analysis [illegible] is used. This is based on the finite [illegible] by Yee

---

[illegible]

System for Banking Environment 1993 IEEE .
16. D. A. Pender. "Neural Networks and Handwritten Signature Verification.", PhD Thesis, Department of Electrical Engineering, Stanford University, 1991.
17. Clark, T., Hastie and E. Kishon, (1990):A model for comparing signatures.1990 IEEE.
18. M. Ammar. Performance of Parametric and Reference Pattern Based Features in Static Signature Verification: A Comparative Study Proc of the 10th Int. Conf on Pattern Recognition, Atlantic City, New Jersey, Vol I, pp. 646-648,1990.
19. Maan Ammar, Yuuji Yoshida and Teruo Fukumura, "Structural Description and Classification of Signature Images", Pattern Recognition, Vol 23, No.7, pp. 697-710,1990
20. Ramannjan, S. Kashi, William Turin and Winston L.Nelsonn (1996): On-Line handwritten signature verification using stroke direction coding. Opt. Eng. 35(9) 2526-2533 (September 1996).
21. Takenovu Matsnura and Seiji Okamura, "On FIR Filter for Signature Verification", in the proceedings of the 38th Midwest Symposium on Circuits and Systems, 1996 IEEE.
22. Mark J. Paulik and N. Mohankrishnan (1993): A 1-D, Sequence Decomposition Based, Antoregresive Hidden Markov Model for Dynamic Signature Identification and Verification, 1993 IEEE. Press, W.
23. H. Chang, J. Wang, and H. Suen., " Dynamic Handwritten Chinese Signature Verification.", Proc Second Int Conf on Document Analysis and Recognition, pp. 258-261, Oct 1993.
24. T. Hastie, E. Kishon, M. Clark and J. Fan. "A Model for Signature Verification." Proc IEEE Int Conf on Systems, Man, and Cybernetics, Oct 13-16, 1991, Charlottesville, pp. 191-196
25 Quen-Zong Wu, I-Chang Jou, and Suh-Yin Lee, "On-Line Sognature Verification Using LPC Cepstrum and Neural Networks ", IEEE Trans. On Systems, Man and Cybernetics-Part B: Cybernetics, Vol. 27, No. 1, February 1997.
26. L. Claesen, D. Beullens, R. Mariens, R, S. De Schrijver, W. de. Jong, " SmartPen: An Application of Integrated Microsystem and Embedded Hardware / Software CoDesign", ED&TC'96 User Forum, pp. 201-205,1996.
27. Yang Xuhua, Takeshi Furuhasi, Kenzo Obata and Yoshiki Uchiakawa, "Constructing a High Performance Signature Verification System Using a GA Method", 1995 IEEE.
28. Higashino, J. (1992): Signature Verification System on Neuro-Computer, .11th IAPR Int. Conf. on PR., 1992.
29 M. Parizeau and R. Plamondon. "A comparative Analysis of Regional Correlation, Dynamic Time Warping, and Skeletal Tree Matching for Signature Verification". Trans on Pattern Analysis and Machine Intelligence, Vol 12, No 7, pp710-717, 1990.
30. Lorette, G. (1984): On-Line Handwritten Signature Recognition Based on Data Analysis and Clustering. Proceedings of the 7th Int. Conf. on Pattern Recognition, Montreal, Canada, July 30, 1984.
31. Forgers Beware, im Neural Edge Issue 7 - Autumn 1994
32 Lo, Z. P. , Yaoqi Yu and Bavaria B. (1993): Analysis of the convergence Properties of Topology Preserving Neural Networks IEEE Trans. on NeuralNetworks, VOL. 4, NO. 2, March 1993.
33. Fairhurst, M. C. and Brittan, P. (1992) : A Parallel Algorithm to Individually Optimized Handwritten Signature Verification.1992 IEEE.
34. 5th Glove'95 User's Manual, 5DT,Fifth Dimension Technologies, Version 1.0- January, 1996.
35 Kohonen (1990): The Self-Organizing Map, Proceedings of the IEEE, VOL. 78, NO. 9. September, 1990.
36. Bezdek, J. C.and Pal, N. R. (1995): A Note on Self-Organizing Semantic Maps, IEEE Trans. On Neural networks, pp. Vol. 6, No. 5, September.
37. Fausett. L. (1994) : Fundamentals of Neural Networks' Prentice Hall,1994.
38. M. Turk and A. Pentland, Eigenfaces for Recognition, J. Cognitive Neuroscience, vol. 3, no.1. pp. 71-86,1991.

reducing the signature data dimensionality from 80 samples to 10 values significant components. The most discriminant eigenvalues are selected to achieve the best signal representation in the reduced dimensionality space. The first ten principal components have been enough to discriminate all signatures correctly. In a third experiment, the interclass correlation coefficients are used with a SOFM. The performance in this case is 95% correct recognition. A comparative study is performed between the three techniques. Results of comparison show that combining the 21 correlation features, with the 6 x 10 eigenfeatures results in zero error with 100% confidence. Although, experimental results demonstrated that the proposed system is highly effective, it should be validated on a large signature database. The cooperative classifier group implemented in this paper enhance the performance of the system. Further work is needed to study the effect of the individual glove signals on the overall system performance. Although preliminary investigations demonstrate the effectiveness of the proposed technique in rejecting skilled forgeries, reliable statistics on the false rejection and false acceptance rates of the overall procedure require the gathering of a much larger database. Alternative approaches could be implemented for solving the problem of variable signature length like interpolation or down-sampling to adjust the length of signals to the size of the input layer of a neural network.

Acknowledgments

The author would like to thank the signers who provided the initial data for this work.

9. References

1 Abu-Rezq A. and Tolba, A. S., Coopemtive Self-Organizing Maps tor Signature Verification, in the Proceedings of the International Workshop "IAIF'97: Image Analysis and Information Fusion", 6-8 November, 1997, Adelaide, Australia, pp.391–402.

2. Plamondon and G. Lorette. "Automatic Signature Verification and Writer Identification - The State of the Art". Pattern Recognition, Vol 22, pp. 107-131, 1989.

3. F. Leclerc and R. Plamondon, "Automatic Signature Verification: The State of the Art - 1989-1993" in International Journal of Pattern Recognition and Artificial Intelligence, Volume 8, Number 3. Singapore, June 1994, pp. 643-660.

4. R. Plamondon. "The Design of an On-line Signature Verification System: From Theory to Practice" In International Journal of Pattern Recognition and Artificial Intelligence, Volume 8, Number 3. Singapore, June 1994.

5. Kai Huang and Hong Yan, "Off-Line Signature Verification Based on Geometric Feature Extraction and Neural Network Classification", Pattern Recognition, Vol. 30, No. 1, pp. 9-17, 1997.

6. Reena Bajaj and Santanu Chaudhury, "Signaturu Verification Using Multiple Neural Classifiers", Pattern Recognition, Vol. 30, No. 1, pp. 1-7, 1997.

7. Robert Sabourin, Ginette Genest, and Francoise Preteux, "Pattern Spectrum as a Local Shape factor for Off-Line Signature Vurification", in IEEE Transactions on Pattern Analysis and Machine Intelligence, VOL. 19, NO 9, September 1997, pp. 976-988.

8. Drouhard, J. P; Sabourin, R. and Godbout, M. (1996) : A Neural Network Approach to Off-Line Signature Verification Using Directional PDF, Pattern Recognition, Vol. 29. No. 3, pp. 415–424, 1996.

9 Wen, C. and Jeng B. (1996): Optimal segmentation of handwritten Chinese signatures using wavelet transforms, Opt. Eng. 35/9, 2721-2729 (September 1996)

10. Lee, L. L and Lizarraga, M. G (1996): Off-Line Methods for Human Signature Verification, Proceedings of the IASTED Int. Conf. Signal and Image Processing (SIP'96), 1966, Florida, USA.

11. Darwish, A. M. and Auda, G. A. (1994): A New Composite Feature-Vector for Arabic Handwritten Signature Recognitiou, Proc IEEE Int Conf ou Acoustics, V2 . 1994, pp 613-666.

12. Isabelle Pottier and Gilles Burel, "Identification and Authentication of Handwrinen Signatures with a Connectionist Approach", 1994 IEEE.

13. Y Qi and B. R Hunt. "Signature Verificatiou using Global and Grid Features. Patteru Recognition", Vol 27, No 12, pp 1621-1629, Dec 1994.

14. Qi Y. and Hunt B.R. (1993): Verification of Handwritten Signature Images by Multiresolution Wavelet Analysis.1993 IEEE.

15. Hui, Sui-Cheung and Teo Wee-Chong (1993) The Design of an Intelligent Signature Processing

Table 4 shows the responding neurons for each of the 6 signals in a training set acquired from 20 persons and represented with the first ten principal components. (Average training time is about 1 Minute, on a 200 MHz MMX Pentium).

	F1	F2	F3	F4	F5	F6
1	54	73	69	44	11	18
2	28	20	21	7	53	69
3	69	3	2	75	22	3
4	61	32	12	67	6	27
5	45	50	74	26	4	57
6	63	27	10	71	12	17
7	31	56	26	13	42	75
8	65	11	7	60	16	10
9	39	18	31	11	45	76
10	22	59	18	1	40	72
11	53	30	9	63	10	19
12	7	76	4	57	29	6
13	51	7	6	49	18	9
14	76	25	1	76	25	1
15	73	1	2	74	24	2
16	34	63	46	19	37	73
17	48	39	62	66	7	25
18	57	44	14	69	1	33
19	58	67	76	31	3	64
20	1	35	6	52	14	12
PCC	100%	100%	95%	100%	100%	100%

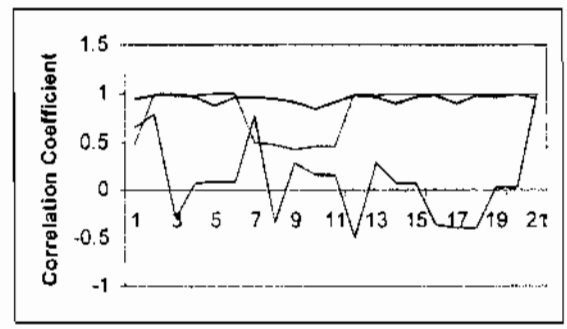

Figure 11. Linear Correlation Coefficients for Three Different Signers

8. Conclusions and Future Research

In this paper, we described a new real-time system for the recognition of virtual hand signatures. To the best author knowledge, this is the first time, that a data glove is used as a signature input device. Signatures are reliably recognized. Both the self-organizing feature map and the principal component analysis technique are used for data reduction. In a first experiment, a 1D-self-organizing map is used to map an input signature of 80 samples onto only one output neuron. The PCA is used in a second experiment for

Table 3 shows the responding neurons for each of the 7 signals in a training set from 20 persons.
(Average training time: about 13 Minutes, on a 200 MHz MMX Pentium

	F1	F2	F3	F4	F5	F6	F7
1	34,40	1,2	19,20	22,24	[illegible]	[illegible]	1,19
2	5,6	22	6	4	[illegible]	[illegible]	41
3	47,48	42	29	47,48	[illegible]	[illegible]	55
4	60,61	58,62	53,56	16,17	[illegible]	15	49,50
5	21,22	28,29	11,12	9	[illegible]	6	7
6	71,76	74,76	60,73	17,36	[illegible]	[illegible]	21,23
7	4,59	17,34	4,41	1,20	[illegible]	[illegible]	17,47
8	65,67	39,50	38,39	32,33	[illegible]	[illegible]	45,46
9	1	20,21	1	2	[illegible]	[illegible]	1
10	25,26	15,16	8	6	[illegible]	[illegible]	29
11	38,39	60,64	64,66	35	[illegible]	[illegible]	63
12	13,14	5,6	24,25	40,41	[illegible]	[illegible]	59,60
13	42,43	36,37	34,37	40,41	[illegible]	[illegible]	15,17
14	50,55	68,70	27,28	27,29	[illegible]	[illegible]	73,76
15	52,54	44,45	30,31	45,51	[illegible]	[illegible]	68,69
16	3,37	1,14	2,21	56,63	[illegible]	[illegible]	13,35
17	32,35	51,54	43,50	3,25	[illegible]	[illegible]	10,12
18	30	31,32	46,47	18,19	[illegible]	[illegible]	51,52
19	28,30	9,10	16,45	14	[illegible]	[illegible]	1,2
20	16,17	48,56	35,36	11,13	[illegible]	[illegible]	15,16
PCC	97.5 %	97.5%	100%	100%	[illegible]	[illegible]	97.5

Underlined pattern numbers are miss-classified.

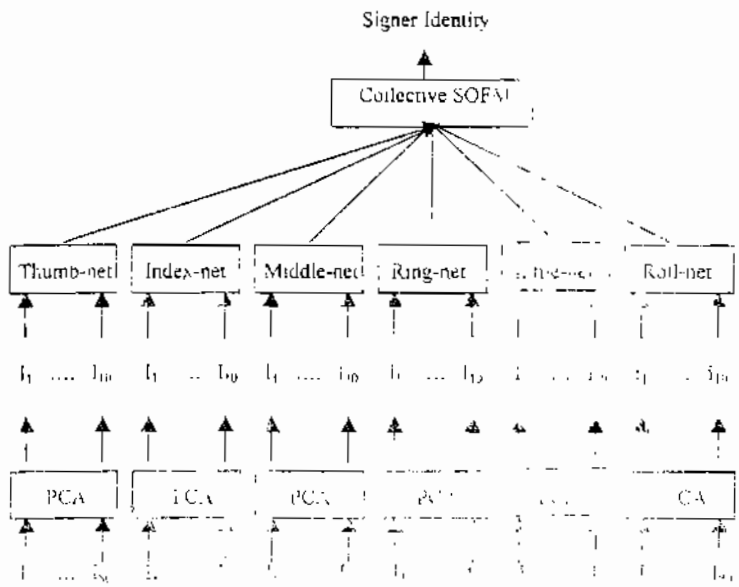

[illegible]

represented with the first ten principal components. The average training time for each SOFM is about 1 Minute, on a 200 MHz MMX Pentium based machine which is too much faster than the first experiment. The classification performance (PCC) of the individual classifiers ranged from 95% to 100%. A cooperative set of classifiers is used to build a democratic classifier that uses a weighed voting technique resulted in a zero error rate. The performance of the PCA and SOFM based approach is better than that of the approach based only on the SOFM and is computationally less expensive.

7.3 Effect of within Class Features and Signing Time on Classifier Performance

Another thing that needs to be investigated is how system behaves as certain aspects such as the signing time and interclass correlation is considered. The linear correlation between the seven glove signals is computed and used for training the SOFM for further data reduction. Seven signals are used to compute a correlation matrix of dimension 7 x 7. The seven diagonal elements are neglected. Since the correlation matrix is symmetric, only 21 correlation coefficients could be considered. For a pair of feature vectors (x_i,y_i), I=1,...,N, the linear correlation coefficient r is given by the formula (6)

$$r = \frac{\sum_{i=1}^{n}(x_i-\bar{x})(y_i-\bar{y})}{\sqrt{\sum_{i=1}^{n}(x_i-\bar{x})^2}\sqrt{\sum_{i=1}^{n}(y_i-\bar{y})^2}} \qquad (6)$$

Where, $\bar{x}$ is the mean of the x_i's and $\bar{y}$ is the mean of y_i's. The 21 coefficients are used as a one-dimensional feature vector for training the self-organizing feature map. An experiment performed on 20 persons with two signatures per person resulted in a correct verification rate of 95.00 %. Fignre 11 shows the distributions of the 21 correlation coefficients for three different signers. This experiment shows the importance of the interclass correlation as a feature set. Combining the 21 correlation features, with the 6 x 10 eigenfeatures results in zero error with 100% confidence.

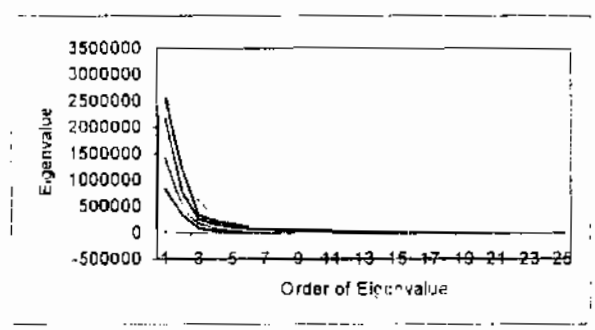

Figure 7: The most discriminant eigenvalues for the six glove signatures

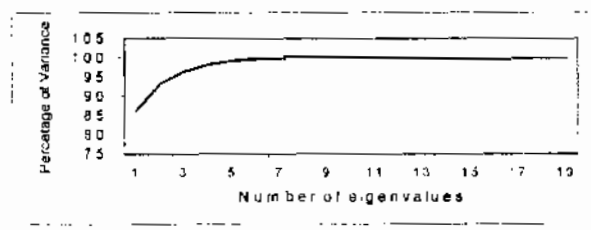

Figure 8: Pereentage of total variance accounted for by a set of eigenvalues

response of the individual SOFMs is fed into the collective SOFM to conduct the identity of the signer. Figure 9 shows the architecture of the classifier based on both the principal components and SOFMs.

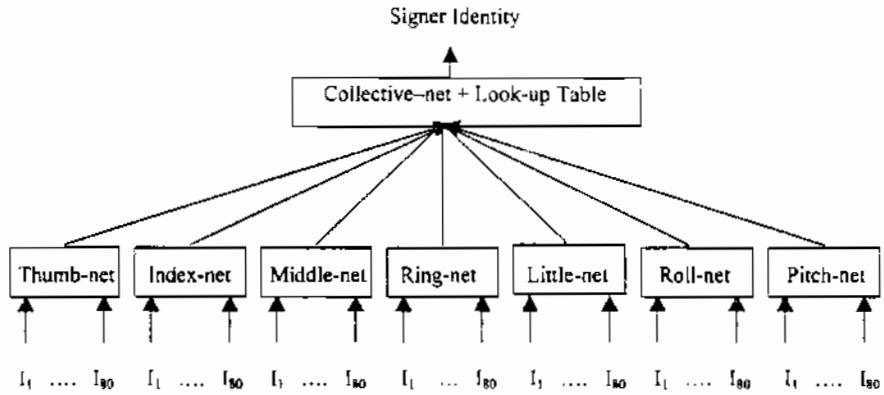

Figure 6: SOFM Based Neural Network Classifier Architecture

7. Experimental Results

In this section, we discuss the results of each of the aforementioned dimensionality reduction techniques and the resulting classification performance. The initial experiments are performed on a signature database consisting of 200 signatures from 20 subjects. This signature database is constructed at Kuwait University using the 5th Glove. The signatures were acquired and sampled at a rate of 300 Hz. Signature data is then down sampled to about 80 samples per signature. A training set is selected to include 100 signatures from 20 writers. The remaining 100 signatures were used for the test purposes.

7.1 Data Reduction Using a Group of Self-Organizing Feature Maps

A set of eight self-organizing feature maps is used. Seven 80-dimensonal feature vectors are used for training the system on each of the five fingers, roll and pitch. Since the length of the feature vectors may vary from one writer to the other, the maximum possible size is conducted from the signature database, and the short vectors are padded with zeros to reach the maximum size in order to solve the problem of the neural network architecture. The cooperative classifier group is integrated using front end classifier with a look-up table.

Table 3 shows the responding neurons for each of the 7 signals in a training set acquired from 20 persons with 2 signatures per person. The average training time for each SOFM is about 13 Minutes, on a 200 MHz MMX Pentium based machine. The classification performance (PCC) of the individual classifiers ranged from 90% to 100%. A cooperative set of classifiers is used to build a democratic classifier that uses a weighted voting technique resulted in a zero error rate. The individual classifier errors could be reduced by increasing the number of neurons per class.

7.2 Signature's Data Reduction Using PCA and SOFM

A second experiment uses the principal component analysis for reducing the high dimensionality feature vectors (80 dimensions) into the most discriminant seven components. In this experiment, the pitch feature-vector is eliminated, as it represents the angle of the signer's hand with respect to the horizontal plane, which is nearly constant along the period of signing and its impact on the recognition process is not high like the other six signals. The reduced space representation for each of the six feature-vectors results in only ten components. The 6 x 10 components represent the whole hand motion (virtual signature). These 60 components mapped on a two dimensional SOFM for further data reduction. Table 4 shows the responding neurons for each of the 6 signals in a training set acquired from 20 persons with 5 signatures per person and

One of the obvious ways to test how well the system works is to simply combine all the feature sets discussed above into one test. In total, 7 feature vectors were used. Since the seven acquired feature vectors with each 80 samples can be treated as high dimensional feature vectors, it was necessary to extract the most discriminant features from each vector.

Given a population of n-dimensional panern vectors $X = [x_1, x_2, x_3, \ldots, x_{n-1}, x_n]^T$, the mean vector of the population id given by:

$$\mu_x = E[X] \tag{1}$$

Where E[X] is the expected value of the pattern vector, X. The covariance matrix of the pattern vector population is defined as:

$$\sum_x = E[(x_k - \mu_k)(x_k - \mu_k)^T] \tag{2}$$

Which is real, symmetric, and on the order of n x n. The elements of the covariance matrix represent the covariance between elements x_i and x_j of the X vector. If x_i and x_j are uncorelated, the covariance is zero. The eigenvectors V of the covariance matrix and their corresponding eigenvalues are used to construct a reduced dimentionality representation of the input patterns. Since we expect that a relatively small number of features are sufficient to characterize a signature class, it is efficient and reasonable to approximate the feature space X using m < n columns of V to give

$$\hat{X}(m) = \sum_{i=1}^{m} y_i v_i \tag{3}$$

The vi's are the column vectors, the best vectors which are associated with the m largest eigenvalues of the covariance matrix of X. The reduced feature space can be easily computed from

$$R_i = v_i^t (X - \bar{X}), i = 2, \ldots, m \tag{4}$$

To determine m, the number of features in the reduced space, we first rank the eigenvalues in a decreasing order. The principal components which correspond to the most significant eigen components are retained according to the following criterion (5):

$$\frac{\sum_{i=1}^{m} \lambda_i}{\sum_{j=1}^{n} \lambda_j} \rangle p \tag{5}$$

Such that P indicates the percentage of variance retained in the selected components. The less significant components are rejected. It is found that the first largest ten eigen components encompass about 99.995% of the total variance of the original signals. Therefore, the feature set of 80 samples is reduced to only ten significant features. The whole virtual signature is represented by a highly disriminant feature vector of dimension 70. Figure 7 shows the magnitudes of the most significant eigen values for the six feature vectors. Figure 8 shows that the first principal component accounts for 87% of the total variance of the data representing the first finger in this purticular example. The first ten principal components account for 99.995 % of the total variance.

6. Dimensionality Reduction Using Both PCA and SOFMs

A second experiment uses the principal component analysis for reducing the high dimensionality feature vectors (80 dimensions) into the most discriminant components. The reduced space representation for each of the six feature vectors results in only ten components. The 6 x 10 components represent the whole hand motion. These 60 components are mapped onto 6 one-dimensional SOFMs for further data reduction. The

5. Methods for Dimensionality Reduction of Virtual Signature's Data

In this section we examine two feature dimensionality reduction techniques for solving the signature recognition problem by comparing two methods, namely the self-organizing map alone, and the combined PCA with the self-organizing maps. A set of features appeared to individually, be good discriminants between signatures.

5.1.1 Dimensionality Reduction Using a Group of Self-Organizing Feature Maps

Neural networks have been shown to be a powerful paradigm for solving many pattern recognition problems. Self-organizing feature maps are widely used in many applications. In the self-organizing process, we are aiming at mappings which transform a signal pattern of arbitrary dimension n onto a one or two-dimensional array. Kohonen's topology-preserving map creates a representation of a multidimensional sensory space on a grid of neurons. Neighboring areas in the sensory space are mapped to neighboring areas on the neural grid. The mapping takes place through a learning process. The learning phase of the feature map is an iterative procedure in which each iteration has three steps: the presentation of a randomly chosen input vector from the input space, the evaluation of the network, and an update of the weight vectors. The details of the SOFM algorithm could be found in [37].

The main problem in training the self-organizing maps is the large variation in the period of signing. A second problem is the intra-personal variations from time to time. This requires solving the problem of determining the most suitable number of neurons in the input layer. The optimum input layer size is specified according to studies performed on many different signatures for a specific sampling rate. The shortest and longest signatures are used to conduct an optimal window size whose maximum limit is specified by the longest possible signature. The short signatures are padded with zeros to reach the maximum window size (mostly longer than all signatures encountered in the training process). The maximum duration of a signature determines the size of the buffer.

This section applies a combined classifier of 8 self-organizing feature map (SOFM) [35-37] to the automatic classification of virtual signatures. Seven feature vectors are first acquired from the hand glove in real-time. The topology preserving feature mapping algorithm clusters the input feature vectors of a training set onto the network structure. A set of eight 1D self-organizing feature map classifiers is used. Seven feature vectors are used for training the system on each of the five fingers, roll and pitch. Since the length of the feature vectors may vary from one writer to the other, the maximum possible size is conducted from the signature database, and the short vectors are padded with zeros to reach the maximum size in order to solve the problem of the neural network architecture. The cooperative classifier group is integrated using a weighed voting technique.

Each SOFM includes an input layer of 80 neurons (size of input vector) and an output layer of 77 neurons (experimentally conducted). Figure 6 shows the architecture of the combined classifier used for signature recognition. A training set of 105 signatures is used for system training. The learning phase of the feature map is an iterative procedure in which each iteration has three steps: the presentation of a randomly chosen input vector from the input space, the evaluation of the network, and an update of the weight vectors. Details of the SOFM training algorithm are to be found in [1]. Neighboring neurons in the network represent neighboring locations in the feature space. The self-organizing map is trained to cluster the training set consisting of a number of virtual signature's vectors of dimension 80. Each signature class is assigned about 4 neurons, which means that there is a specific set of neurons which respond to the input signatures of a specific signer. After the training clusters are formed. The output clusters of the individual 7 SOFMs are collected and fed into a collective set of SOFM for identification of the signers identity using a simple look-up table.

5.2 Principal Component Analysis (PCA)

The principal component analysis method is extensively used in the field of face recognition. The method is well known as Eigenface method [38]. An analogous method is proposed in this paper; that is the Eigensignature method. The Eigensignature method is based on linearly projecting the signature space to a low dimensional space. The resulting projections maximize the scatter across all classes, i.e., across all signatures of all signatures.

3. Glove Bascd Acquisition of Signature Data

Glove signature data is acquired using a 8-bit resolution (256 positions) for each finger as well as for the axes of the tilt sensor (roll and pitch). The 5th Glove'95 [34] sensors are based on flexor technology [optical fiber based]. Each finger is fitted with one "sensor" which measures the average flexure of that finger. The full hand (5 fingers, roll angle, pitch angle) may be sampled up to 200 times every second. The roll and pitch angles of the glove are measured using a tilt sensor through a +/- 60 degree linear range. The tilt sensor is mounted on the glove with a velcro strip. The 5th Glove starts up in command mode. Serial information is accepted and transmitted using 19200 baud, 8 bits, 1 stop bit, no parity through a serial link that utilizes the TX, RX and GND lines. No handshaking is defined. The glove has a 1-byte input buffer. The acquired data for signature recognition lasts several seconds. The correlation between the input sensors is unknown. All seven input signals were used for recognition. Meaningful signature signals are spotted using a variance based technique to locate both the start and end points of a gesture. Another difficulty is the variation of the same gestures in shape and duration depending on the emotional state of the user. Spatial and temporal variations must be considered simultaneously. Figure 2 shows a typical signature on paper and the corresponding seven glove signals (five fingers, roll and pitch) as measured during the signing process. The recorded seven signals represent the bending angles of the five fingers, the roll and the pitch of the signers hand. Each of the seven measured values is recording during the time of the signing process.

4. Signature Dynamics and Sensitivity of Signature to Individual's Hand

Figure 3 shows two examples of the virtual signatures acquired from three subjects. Figure 3 shows the image of a typical signature and its corresponding glove based seven signals. Glove signals acquired during the signing process are completely different for the same looking signatures as shown in figure 3-a. The first signature to the right is the genuine and next is the skilled forgery. Figure 3-b shows another genuine signature and its corresponding skilled forgery. The signals with dashed lines correspond to the forged signatures.

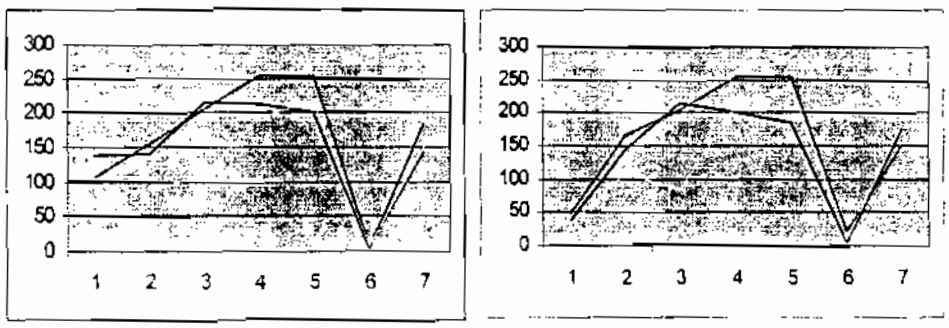

(a) (b)

Figure 4. Two gestures from three persons (a) Fist, (b) Number '1'

To recognize the effect of signers hand shape on the output signals from the data glove, three individuals were asked to repeat two specific hand gestures. Figure 4. shows the two different gestures acquired by the 5th Glove from the three different persons. Although the gestures are the same, individual's hand size have a very clear impact on his gesture. This phenomenon is preferable in applications such as signature recognition. Using a data glove as a signature acquisition device helps considering both the hand size and the dynamics of hand motion in the signing process.